

Photoinduced cleavage by a rhodium complex at G·U mismatches and exposed guanines in large and small RNAs

Christine S. Chow ^{a,*}, Philip R. Cunningham ^b, KangSeok Lee ^b, May Meroueh ^a, John SantaLucia Jr. ^a, Shikha Varma ^a

^a Department of Chemistry, Wayne State University, Detroit, MI 48202, USA

^b Department of Biological Sciences, Wayne State University, Detroit, MI 48202, USA

Received 22 February 2002; accepted 28 March 2002

Abstract

Photoinduced cleavage reactions by the rhodium complex tris(4,7-diphenyl-1,10-phenanthroline)rhodium(III) {Rh(DIP)₃³⁺} with three RNA hairpins, r(GGGGU UCGCUC CACCA) (16 nucleotide, tetraloop^{A1a2}), r(GGGGCUAUAGCUCUAGCUC CACCA) (24 nucleotide, microhelix^{A1a}), and r(GGCGGUUAGAUUCGCC) (17 nucleotide, 790 loop), and full-length (1542 nucleotide) 16S rRNA from *Escherichia coli* were investigated. The cleavage reactions were monitored by gel electrophoresis and the sites of cleavage by Rh(DIP)₃³⁺ were determined by comparisons with chemical or enzymatic sequencing reactions. In general, RNA backbone scission by the metal complex was induced at G·U mismatches and at exposed G residues. The cleavage activity was observed on the three small RNA hairpins as well as on the isolated 1542-nucleotide ribosomal RNA. © 2002 Société française de biochimie et biologie moléculaire / Éditions scientifiques et médicales Elsevier SAS. All rights reserved.

Keywords: Rhodium; Hairpin; Cleavage; Chemical probing; 16S rRNA

1. Introduction

A number of organic and inorganic compounds have been shown to induce strand scission of RNA through oxidation of the sugar or base residues. Examples include Fe(EDTA)²⁻ [1], bis(1,10-phenanthroline)copper(I) [2], octahedral complexes of rhodium(III) and oxoruthenium(IV) metallointercalators [3–6], square-planar nickel(II) complexes [7], Fe(II)-bleomycin [8], and nickel(II) metalloproteins [8]. These compounds can serve as site-specific probes of RNA structure, as model systems to understand RNA damage in biological systems, or as potential therapeutic agents.

Previous studies revealed that the metal complex tris(4,7-diphenyl-1,10-phenanthroline)rhodium(III) ([Rh(DIP)₃]Cl₃ or Rh(DIP)₃³⁺, Fig. 1) induces strand scission at nucleotides adjacent to G·U mismatches as well as at exposed G residues in tRNA^{Phe}, tRNA^{Asp}, 5S rRNA, and in smaller

RNA hairpins [3,9]. In all the cases examined, the reaction involved only metal complex and irradiation at 313 nm. No external agents were required and no further alkaline treatment was necessary. Furthermore, not all of the G·U mismatch sites on tRNA were cleaved by Rh(DIP)₃³⁺ (several are protected due to tertiary folding of the RNA), suggesting that close contact between the metal complex and RNA is required. Similarly, (2,12-dimethyl-3,7,11,17-tetraazabicyclo[11.3.1]heptadeca-1(17),2,11,13,15-pentaenato)nickel(II) perchlorate ([NiCR](ClO₄)₂) [7], flavin mononucleotide (FMN), riboflavin, and isoalloxazine derivatives [10,11] also promote cleavage at G·U sites within double-helical regions of RNA. Interestingly, all of these known G·U-cleaving molecules induce strand scission on the 3' side of uridine, which has been characterized as the “destacked” side of the G·U mismatch [12–14]. In contrast to reagents that lead to guanine oxidation or alkylation (alkaline-labile cleavage), the G·U-specific reagents all cleave by mechanisms involving direct strand scission.

Here, we extend these studies to examine cleavage reactions on three other RNAs in which G·U mismatches have functional roles, such as *Escherichia coli* tRNA^{A1a}.

* Corresponding author. Tel.: +1-313-577-2594; fax: +1-313-577-8822.
E-mail address: csc@chem.wayne.edu (C.S. Chow).

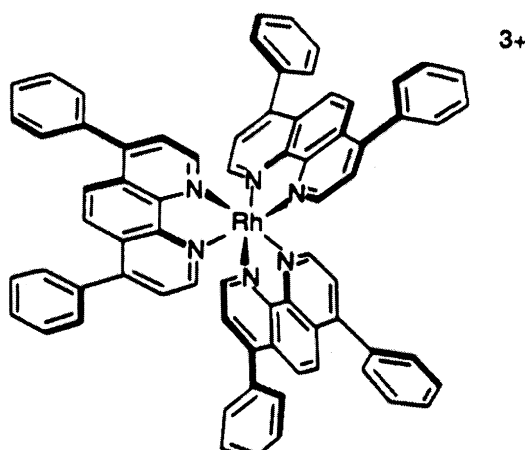


Fig. 1. A schematic representation of $\text{Rh}(\text{DIP})_3^{3+}$ is shown.

Base mismatches in RNA are generally found at biologically significant locations. For example, a G·U pair in *E. coli* tRNA^{Ala} is responsible for recognition of tRNA by its cognate synthetase, AlaRS [15,16]. A G·U pair is also important in ribosomal L32 protein recognition [17] and another is found at the group I intron splice site [18]. The G·U sites in 16S and 23S rRNA are abundant (~120 sites) [13,19], although in most cases, their relationships with RNA function have yet to be established. The G·U wobble pairs can exist in many different orientations and sequence arrangements [13], and the role of each motif in regulating local RNA secondary structure or mediating RNA and/or protein interactions remains to be determined. Thus, structure probing with compounds such as $\text{Rh}(\text{DIP})_3^{3+}$ serves several roles, such as: (1) identifying and characterizing new G·U motifs in different RNA sequence and secondary structure contexts, and (2) relating these structures to physical and biological properties and functions of RNA in the ribosome.

We have chosen to study the 790-loop region of *E. coli* 16S rRNA because extensive genetic and NMR studies have already been carried out on this sequence [20]. Genetic experiments revealed that the natural A·C pair at positions 787·795 of *E. coli* 16S rRNA can be replaced by a G·U pair and that the resulting mutant ribosomes were >70% functional in vivo. One-dimensional NMR studies on the 790 loop (the sequence shown in Fig. 2 was employed, which is a slight variation of the wild-type sequence) suggested that A·C- and G·U-containing 790-loop RNAs are isostructural [20]. A complete three-dimensional NMR structure of the G·U variant revealed several distinct features such as a G·U wobble pair, a solvent exposed G residue at position 791, and a “flipped-out” U793 residue (J. SantaLucia Jr., S. Varma, unpublished data). Two-dimensional NOESY experiments on the A·C variant showed NOEs and chemical shifts that were similar to those on the G·U variant. The fact, however, that the G·U variant of 16S rRNA was only ~70% functional compared to the wild-type A·C RNA, suggested either minor structural differences between the two RNAs or

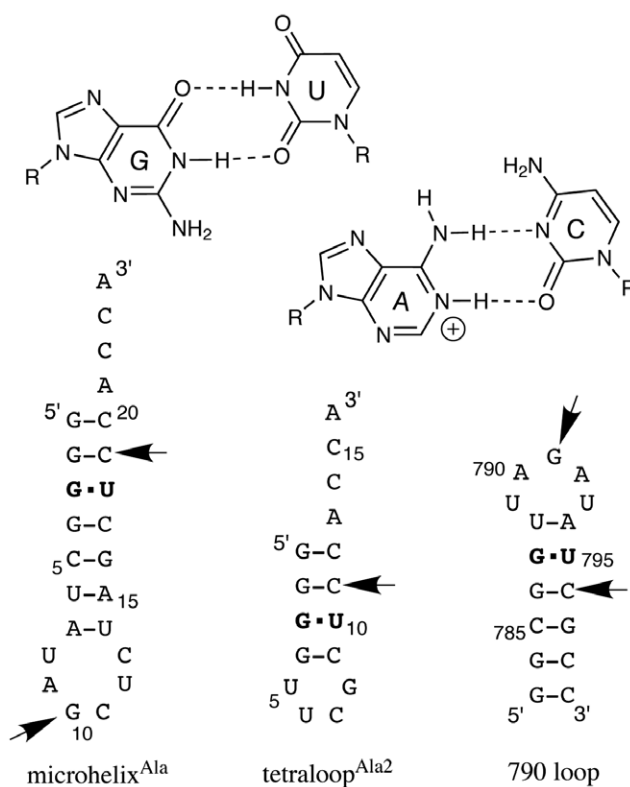


Fig. 2. The three RNA hairpins used in this study are shown. The base-pairing schemes of the G·U and A·C mismatches are shown for comparison. The $\text{Rh}(\text{DIP})_3^{3+}$ cleavage sites are shown by arrows.

different long-range contacts and interactions in the ribosome [20].

The three-dimensional NMR structure of the 790 loop and the crystal structure of the 30S subunit reported by Wimberly et al. [21] show many structural similarities such as a flipped-out U793 on the 3' side of the 790 loop, extensive hydrogen-bonding interactions across the heptanucleotide loop, and base-stacking interactions on the 5' side of the loop. Some differences between the two structures do exist, however, such as different hydrogen-bonding and stacking interactions across the loop and the location of the loop turn (G791 for the NMR structure and A790 for the X-ray structure) [20,21]. The NMR structure clearly shows a stable U788-A794 pair and neighboring stacked wobble pair, whereas the X-ray structure shows unusual single hydrogen bonds between these bases. Possible explanations for the observed differences are: (1) the structure of the natural 16S rRNA with the A·C mismatch is indeed different from the G·U variant, (2) the NMR solution structure of the G·U variant correctly describes the wild-type A·C variant, and crystal packing or other factors play a role in altering the X-ray structure, (3) the presence of proteins or long-range RNA contacts influences the three-dimensional RNA structure in the ribosome and the NMR structure of the 17-nucleotide loop is not an exact representation of the full-length 16S rRNA structure, but does reflect solution dynamics of the loop, or (4) the two structures represent different conformations assumed by the 790 loop during the

protein synthesis process. To examine the structural specificity of the rhodium complex and the significance of the observed differences in the NMR and X-ray structures, the 17-nucleotide 790 loop representing the NMR sequence and the full-length 16S rRNA from *E. coli* were probed with $\text{Rh}(\text{DIP})_3^{3+}$.

2. Materials and methods

2.1. Chemicals, solutions, DNA, and RNAs

All biochemicals and buffer reagents were purchased from either Sigma or Fisher and organics were obtained from Aldrich unless stated otherwise. $[5'\text{-}^{32}\text{P}]\text{pCp}$ was purchased from Perkin-Elmer Life Sciences, Inc. and T4 RNA ligase was obtained from New England Biolabs. RNase-free, distilled deionized water (ddH_2O) was employed for all experiments.

The rhodium compound, tris(4,7-diphenyl-1,10-phenanthroline)rhodium(III) $\{\text{Rh}(\text{DIP})_3^{3+}\}$, was prepared according to the literature [22] and used as a racemic mixture. Stock solutions (1 mM) containing the rhodium complexes were prepared in ethanol and concentrations determined by using ϵ_{296} of 116 000/M/cm. The $\text{Rh}(\text{DIP})_3^{3+}$ stock solutions were stored in the dark at -20°C and diluted in ddH_2O just prior to use.

A single-stranded DNA, d(ACCAAGTCGACATCGTTT) (18 nucleotide, primer 1), was synthesized on a Cruachem PS250 DNA/RNA synthesizer using standard DNA phosphoramidite chemistry. The single-stranded RNAs, r(GGGGUUCGCUCCACCA) (16 nucleotide, tetraloop^{Ala2}), r(GGGGCUAUAGCUCUAGCUCCACCA) (24 nucleotide, microhelix^{Ala}), and r(GGCGGUUAGAU-AUCGCC) (17 nucleotide, 790 loop), were synthesized on a Cruachem PS250 DNA/RNA synthesizer using standard 2'-*O*-Fpmp or 2'-*O*-silyl RNA phosphoramidites and deprotected according to the literature procedures [23,24]. The DNA and RNA hairpins were purified by using polyacrylamide gel electrophoresis (15%, 19:1 acrylamide/bisacrylamide, 7 M urea, 42 cm long \times 0.8 mm thick) in $1\times$ TBE (90 mM Tris, 90 mM boric acid, 2.5 mM EDTA, pH 8.3) followed by electroelution in $0.5\times$ TBE in an Amicon CentrilonTM and desalting on Sep-Pak C-18 cartridges (Waters). Aqueous stock solutions of the DNA or RNAs were kept frozen at -20°C . DNA and RNA concentrations were determined spectrophotometrically at 260 nm, where $\epsilon_{260} = 173\,900$, 148 500, 229 200, and 168 300/M/cm (per molecule) for primer 1, tetraloop^{Ala2}, microhelix^{Ala}, and 790 loop, respectively [25].

2.2. RNA labeling and renaturation

The 3' ends of the RNA hairpins were labeled with ^{32}P by using $[5'\text{-}^{32}\text{P}]\text{pCp}$ and T4 RNA ligase according to the literature procedures (typically 20 pmol of RNA were la-

beled in each reaction) [26]. The labeled RNAs were repurified on 20% polyacrylamide gels (19:1 acrylamide/bisacrylamide, 7 M urea, 42 cm long \times 0.8 mm thick) and electroeluted. The labeled RNAs were stored in 10 mM Tris-HCl, at pH 7.0, and renatured by heating to 70°C for 10 min and slowly cooling to room temperature.

2.3. RNA cleavage reactions

A typical 45 μl cleavage reaction contained 40 000 cpm of labeled RNA, 20–100 μM “carrier”, or unlabeled, RNA (RNA hairpin or yeast tRNA^{Phe}), and 20–100 μM $\text{Rh}(\text{DIP})_3^{3+}$ in 20 mM sodium cacodylate, at pH 7.0, and 50 mM NaCl. The sample was placed in a 50 μl quartz cuvette and irradiated at 313 nm for 5–45 min using a spectrofluorimeter (a 1934D phosphorimeter from SPEX was employed; Fluorolog-2 series with a 1000 W UV xenon flash tube as the light source; the wavelength was set by the monochromator with the slits at 8.0). After the irradiations were complete, the reactions were quenched by freezing on dry ice and the samples were then dried in vacuo. The reaction products were analyzed by co-electrophoresing with diethylpyrocarbonate (DEPC) and hydrazine sequencing reactions [27] on high-resolution 20% (19:1 acrylamide/bisacrylamide), 7 M urea, 42 cm long \times 0.2 mm thick polyacrylamide gels.

2.4. Chemical-probing reactions on 16S rRNA

16S rRNA was isolated from *E. coli* by previously reported methods [28] and renatured in 10 mM Tris-HCl, 10 mM MgCl_2 , and 300 mM KCl, at pH 7.0 by heating to 80°C for 2 min followed by slow cooling (>30 min) to room temperature. The reaction volume was 45 μl and contained 3 μM 16S rRNA, 3.3 μM $\text{Rh}(\text{DIP})_3^{3+}$, 20 mM sodium cacodylate, at pH 7.0, and 50 mM NaCl. The reaction mixture was irradiated for 40 min at 313 nm using the fluorimeter as described in the previous section. The reactions were quenched by the addition of 200 μl 0.3 M sodium acetate, at pH 4.5, and 600 μl EtOH and freezing on dry ice. An RNA pellet was obtained by centrifugation and washed three times with 70% EtOH. DNA primer 1 was 5'-end labeled with $\gamma\text{-}^{32}\text{P}$ ATP and T4 polynucleotide kinase followed by polyacrylamide gel purification (20%, 19:1 acrylamide/bisacrylamide, 7 M urea) in $1\times$ TBE and electroelution. The cleavage products were then determined by using reverse transcriptase and DNA primer 1, which annealed to residues 814–831 on the 16S rRNA. The reverse-transcriptase reactions were carried out according to the literature procedures [29] and employed 20 pmol each of 16S rRNA and DNA primer 1. The reaction products were analyzed by co-electrophoresing with enzymatic sequencing reactions with ddNTPs.

For all chemical-probing studies, the product bands were identified by using autoradiography or by imaging on a

Molecular Dynamics phosphorimager and quantitated using ImageQuant software.

3. Results

3.1. Cleavage of microhelix^{Ala} and tetraloop^{Ala2} RNAs

The initial goal of the work was to identify sites of Rh(DIP)₃³⁺-induced strand scission on mismatch-containing RNAs representing the acceptor stem of *E. coli* tRNA^{Ala}. These RNAs were developed in Schimmel's laboratory as substrates for aminoacyl tRNA synthetases that use the G·U mismatch as a major determinant for aminoacylation specificity [30,31]. A 24-nucleotide RNA hairpin with a single G·U mismatch in the stem region, microhelix^{Ala} (Fig. 2) [30], and 20 μM Rh(DIP)₃³⁺ were irradiated for 10–50 min, with optimal cleavage occurring at 20 min. As shown in Fig. 3A (lanes 2 and 3), strand scission occurred on the 3' side of the G·U mismatch at C19 after 20 min of irradiation. A combination of non-specific cleavage by the metal complex and nuclease degradation was observed in the upper region of the gel (bracketed). The non-specific cleavage increased with longer times of irradiation (50 min), which led to a reduction of the specific cleavage at C19. Minor cleavage was also observed at G10. No cleavage at C19 or G10 was apparent when RNA only (no metal complex) was irradiated (lanes 4–6), or when RNA was treated with rhodium complex in the absence of light (lanes 7 and 8). Further treatment with aniline did not alter the cleavage patterns for either the light controls or for the metal reactions (data not shown), suggesting that damage was mediated at the sugar moiety rather than at the RNA base.

The Rh(DIP)₃³⁺ cleavage products migrated with Peattie sequencing reactions, demonstrating that strand scission likely occurred through release of both 3' and 5' phosphate ends [27]. Previous studies suggested that upon irradiation, certain rhodium(III) polypyridal complexes have the ability to abstract sugar protons (e.g., C3'–H or C1'–H) and cause the nucleotide to further decompose through both base and phosphate release [4,32]. This reaction mechanism differs from a guanine-oxidation pathway that requires alkaline treatment to reveal the damaged site [7].

The microhelix^{Ala} RNA was very sensitive to nuclease degradation and light damage, therefore experiments were repeated with a more stable 16-nucleotide RNA hairpin, tetraloop^{Ala2} (Fig. 2) [31]. Upon treatment with Rh(DIP)₃³⁺ and only 5 min of irradiation at 313 nm, strong cleavage of tetraloop^{Ala2} was observed at C11, which lies on the 3' side of the uridine of the single intrahelical G·U mismatch (Fig. 3B, lanes 1–5). A variety of conditions were employed in which the RNA concentration ranged from 20–100 μM (in molecules), and the RNA was either heat denatured and renatured by slow cooling or used without any refolding. We have observed previously from UV and circular dichro-

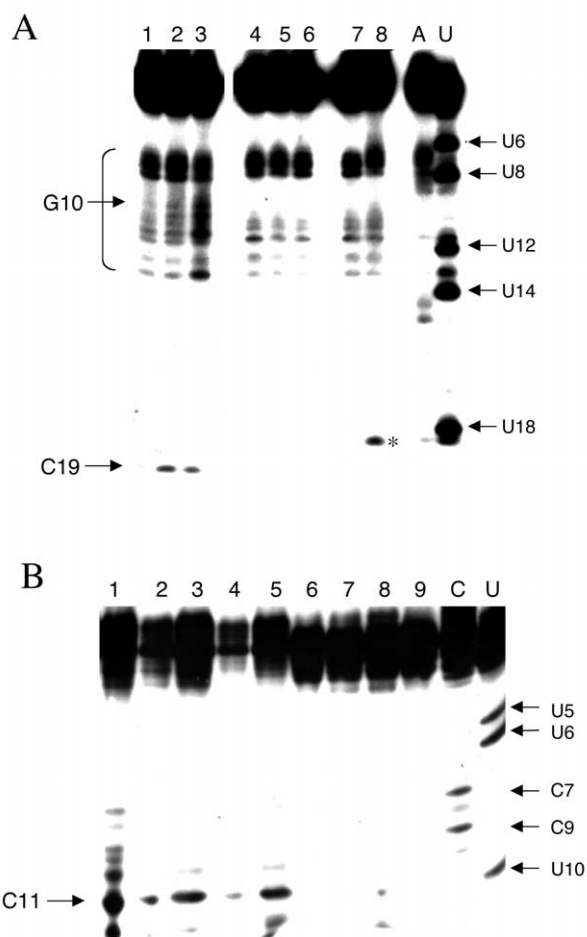


Fig. 3. Cleavage of microhelix^{Ala} (A) and tetraloop^{Ala2} (B) by Rh(DIP)₃³⁺ is shown. (A) Lanes 1–3 (cleavage reactions): <2 pmol ³²P-3'-labeled microhelix^{Ala}, 20 μM Rh(DIP)₃³⁺, and 50 μM carrier RNA (unlabeled tRNA^{Phe}) irradiated at 313 nm for 10, 20, or 50 min, respectively. Lanes 4–6 (light controls): <2 pmol ³²P-3'-labeled microhelix^{Ala} and 50 μM tRNA^{Phe} irradiated at 313 nm for 10, 20, or 50 min, respectively. Lanes 7 and 8 (dark controls): <2 pmol ³²P-3'-labeled microhelix^{Ala}, 20 μM Rh(DIP)₃³⁺, and 50 μM tRNA^{Phe} incubated for 10 or 50 min, respectively. Lane A: DEPC (A-specific) sequencing reaction. Lane U: hydrazine (U-specific) sequencing reaction. The bracketed region and (*) highlight nuclease sensitive sites. (B) Lanes 1–3: <2 pmol ³²P-3'-labeled tetraloop^{Ala2} (no renaturation step), 20 μM Rh(DIP)₃³⁺, and 20, 50, or 100 μM carrier RNA (unlabeled tRNA^{Phe}), respectively, irradiated at 313 nm for 5 min. Lanes 4–5: <2 pmol ³²P-3'-labeled tetraloop^{Ala2} (renatured), 20 μM Rh(DIP)₃³⁺, and 10 or 20 μM tRNA^{Phe}, respectively, irradiated at 313 nm for 5 min. Lanes 6–9: light controls with <2 pmol ³²P-3'-labeled tetraloop^{Ala2} (only lanes 8 and 9 were renatured), and 10 μM (lanes 6 and 8) or 20 μM (lanes 7 and 9) tRNA^{Phe} irradiated at 313 nm for 5 min. For both (A) and (B), arrows on the left indicate cleavage sites and arrows on the right show the sequence assignments.

ism studies that the tetraloop is folded even without the renaturation step [33]. Some additional cleavage near C11 was observed on the lower concentration (20 μM) RNA sample that did not undergo the renaturation step (Fig. 3B, lane 1), suggestive of non-specific interactions, whereas a small amount of light damage was observed on the renatured RNA at lower concentrations (lane 8). The highly

specific cleavage at C11 was not observed on RNA hairpins containing other mismatches at positions 3•10, such as C•A, A•C, G•A, or U•U (data not shown).

3.2. Cleavage of 790-loop RNAs

Similar rhodium-induced cleavage studies were carried out with a 17-nucleotide RNA representing the 790 loop of 16S rRNA (Fig. 2). Light-induced cleavage of the 790 loop by $\text{Rh}(\text{DIP})_3^{3+}$ occurred at the loop residue G791 and at the stem residue C796, which lies on the 3' side of the uridine of the G•U mismatch (Fig. 4A, lanes 2, 3, and 5). Similar cleavage occurred under a variety of conditions

($[\text{Rh}(\text{DIP})_3^{3+}] = 20$ or $40 \mu\text{M}$, $[\text{unlabeled 790-loop RNA}] = 20, 50$ or $100 \mu\text{M}$, irradiation time = 15–45 min; data not shown), although residue C796 was more sensitive towards the reaction conditions (e.g., no cleavage at C796 is apparent in lane 5 of Fig. 4A, in which a higher concentration of rhodium complex was employed). Similar results were obtained regardless of whether the carrier (unlabeled) RNA was yeast tRNA^{Phe} or 790 loop. For the longer irradiation times (45 min), some light-induced damage in the absence of metal complex was observed at the loop residue U789, and was even further enhanced in the presence of $\text{Rh}(\text{DIP})_3^{3+}$.

In order to further define the specificity of the metal complex for base mismatches and exposed residues, six

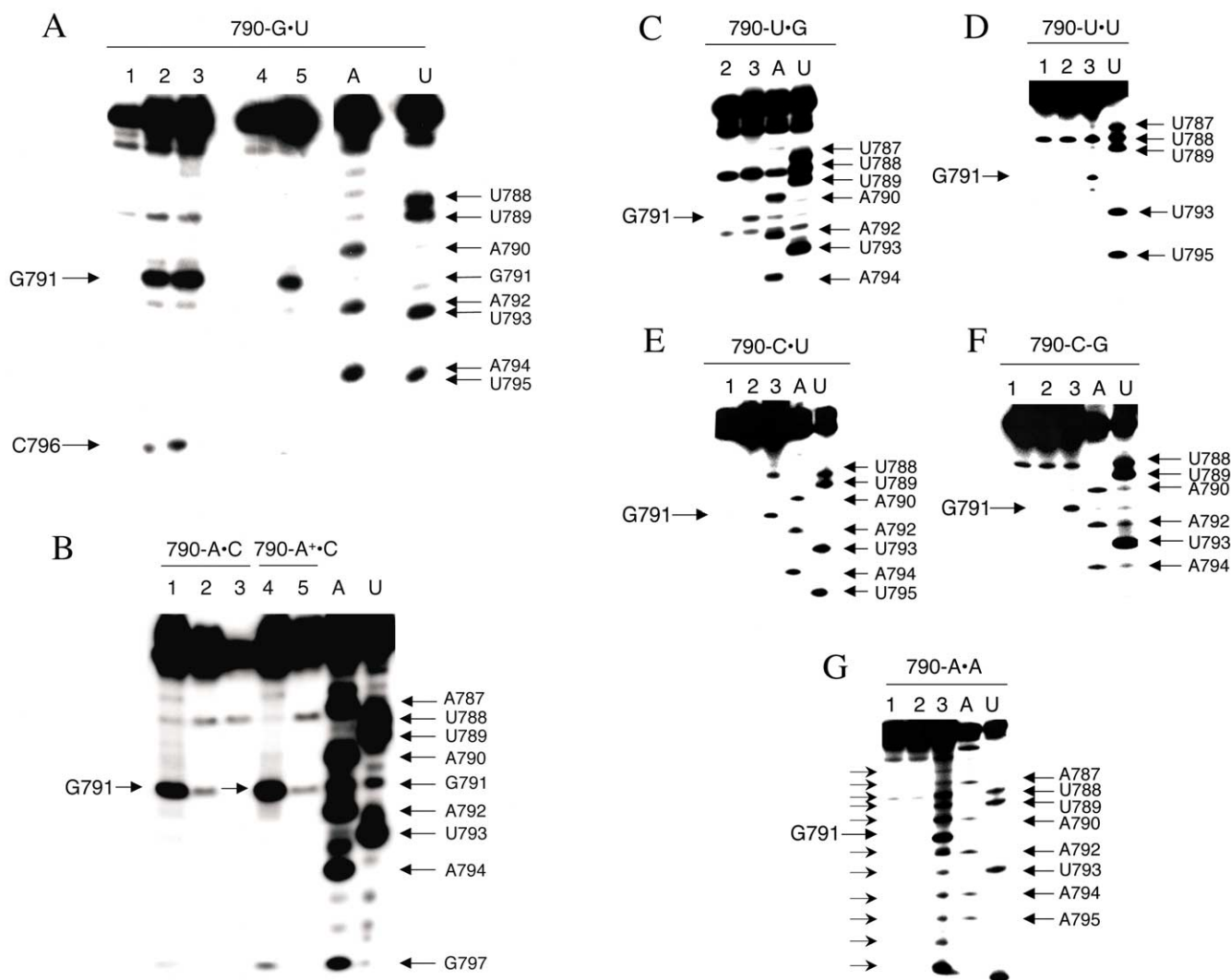


Fig. 4. Strand scission of 790-loop variants by $\text{Rh}(\text{DIP})_3^{3+}$ is shown. (A) Lane 1: $<2 \text{ pmol } ^{32}\text{P-3'}$ -labeled 790 loop (G•U) and $20 \mu\text{M}$ tRNA^{Phe}, irradiated for 45 min at 313 nm. Lanes 2–3, 5: $<2 \text{ pmol } ^{32}\text{P-3'}$ -labeled 790 loop (G•U), 20 (2, 3) or 40 (5) μM $\text{Rh}(\text{DIP})_3^{3+}$, and 20 (2, 5) or 50 (3) μM tRNA^{Phe} irradiated for 45 min at 313 nm. Lane 4: dark control (no rhodium, no light). (B) Lanes 1 and 4: $<2 \text{ pmol } ^{32}\text{P-3'}$ -labeled 790 loop (1 = A•C variant at pH 7.0; 4 = A•A variant at pH 5.0), $20 \mu\text{M}$ $\text{Rh}(\text{DIP})_3^{3+}$, and $20 \mu\text{M}$ unlabeled 790 loop (A•C) irradiated for 20 min at 313 nm. Lanes 2 and 5: light controls. Lane 3: dark control. (C–G) Lane 1: $<2 \text{ pmol } ^{32}\text{P-3'}$ -labeled 790 loop (U•G, U•U, C•U, C•G, and A•A variants, respectively), $20 \mu\text{M}$ $\text{Rh}(\text{DIP})_3^{3+}$, and $100 \mu\text{M}$ unlabeled 790 loop irradiated for 20 min at 313 nm. Lane 2: $<2 \text{ pmol } ^{32}\text{P-3'}$ -labeled 790 loop (U•G, U•U, C•U, C•G, and A•A variants, respectively) and $100 \mu\text{M}$ unlabeled 790 loop irradiated for 20 min at 313 nm. Lane 3: $<2 \text{ pmol } ^{32}\text{P-3'}$ -labeled 790 loop (U•G, U•U, C•U, C•G, and A•A variants, respectively), $20 \mu\text{M}$ $\text{Rh}(\text{DIP})_3^{3+}$, and $100 \mu\text{M}$ unlabeled 790 loop irradiated for 20 min at 313 nm. For (A–G), lane A is the DEPC (A-specific) sequencing reaction, lane U is the hydrazine (U-specific) sequencing reaction, arrows on the left indicate cleavage sites, and arrows on the right show the sequence assignments.

other sequence variants were examined. The 790-loop residues 787-795 were mutated to A•C, U•G, U•U, C•U, C•G, and A•A. These two sites exist as A787•C795 in the full-length 16S rRNA from *E. coli*. Cleavage reactions with $Rh(DIP)_3^{3+}$ were first carried out on the A•C (pH 7.0) and A⁺•C (pH 5.0) 790-loop variants. As shown in Fig. 4B, lanes 1 and 4, strand scission occurred consistently at G791, but not at the base-mismatch site. Minor cleavage was observed at G797, which resides two residues away from the mismatch site. Stronger cleavage at G797 was observed at pH 5.0 compared to pH 7.0, suggesting that protonation of A787 may have some influence on the cleavage at G797. Only cleavage at G791 was apparent on the U•G, U•U, C•U, and C•G 790-loop variants, whereas a series of non-specific cleavages were observed on the A•A RNA variant (Fig. 4C–G, lane 3). Thus, light-induced RNA cleavage by the rhodium complex appears to be specific for G•U mismatches and for exposed G residues, and not for other mismatches, including the A•C (and A⁺•C) pair.

3.3. Cleavage of the 790 loop in *E. coli* 16S rRNA

In order to determine whether the small 17-nucleotide RNA fragment accurately represents the 790 loop in the full-length 16S rRNA, further cleavage studies with $Rh(DIP)_3^{3+}$ were carried out. The 16S rRNA was isolated from *E. coli* ribosomes, then incubated with $Rh(DIP)_3^{3+}$ and irradiated for 40 min at 313 nm. The cleavage sites were identified by annealing a DNA primer at positions 831 through 814 and carrying out reverse transcription of the 16S rRNA. The products were identified by comparison to dideoxy-sequencing reactions. As shown in Fig. 5 (lane 1), one strong and two weaker reverse-transcriptase stop sites occurred. Quantitation of the gel bands revealed that these were indeed the only three sites of rhodium-induced cleavage. Other stop sites are observed, but match the control RNA without added metal complex (lane 2). Thus, one of the limitations of this method is that natural reverse-transcriptase stop sites, light-sensitive sites, or certain modified nucleo

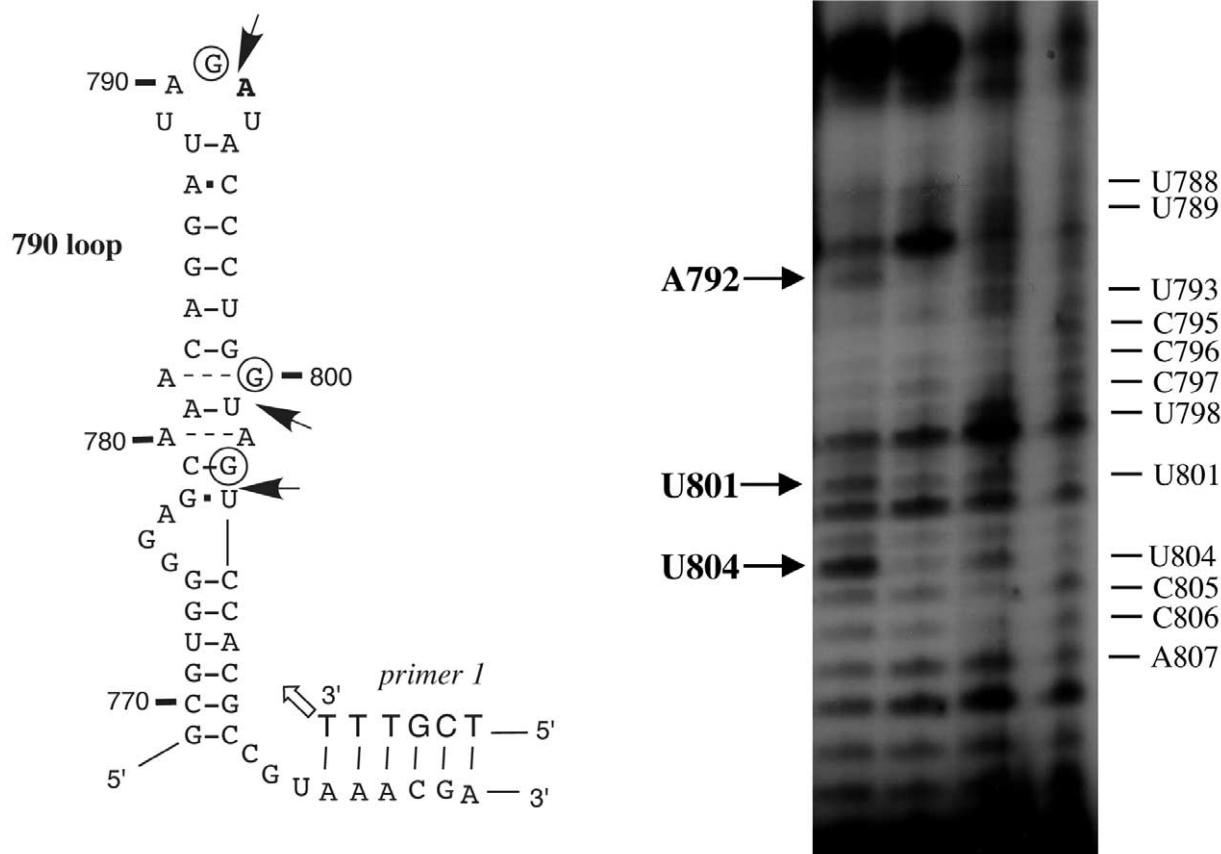


Fig. 5. The secondary structure of 16S rRNA from residues 769–819 is shown on the left; the DNA primer sequence is shown at its annealing site on the rRNA and the direction of reverse transcription is indicated by the open arrow. The $Rh(DIP)_3^{3+}$ reaction sites are indicated by open circles, and the closed arrows reveal sites of strand scission. The autoradiogram for $Rh(DIP)_3^{3+}$ cleavage on the full-length RNA is shown on the right. Lane 1: reverse-transcription reaction of the 16S rRNA (3 μ M) after treatment with 3.3 μ M $Rh(DIP)_3^{3+}$ and irradiation for 40 min at 313 nm. Lane 2: reverse-transcription reaction of the 16S rRNA (3 μ M) after irradiation for 40 min at 313 nm. Lane 3: U sequencing reaction. Lane 4: C sequencing reaction. Arrows to the left of the gel indicate strong stop sites due to cleavage by $Rh(DIP)_3^{3+}$ and the sequence assignment is shown on the right.

sides cannot be identified as rhodium cleavage sites. The three stops occurred at A792, U801, and U804. We assume that cleavage by the rhodium complex will lead to loss of the nucleotide base and release of 5' and 3' phosphates. Thus, the reverse transcriptase would be expected to stop at the base on the 3' side of the rhodium cleavage site. Therefore, the first rhodium cleavage site was identified as G791, the second site as G800, and the third as G803. The first stop site matches the G cleavage site identified on the top of the 17-nucleotide 790 loop, the second occurs at an unusually structured G site, and the third lies on the 5' side of the U of a G·U mismatch at positions 778·804.

4. Discussion

4.1. Cleavage specificity: G·U and exposed-G recognition by $Rh(DIP)_3^{3+}$

$Rh(DIP)_3^{3+}$ is an ideal photocleavage agent to map RNA structure because it has a rigid and well-defined structure that will not be affected by the RNA structure upon binding. On the microhelix^{Ala} and tetraloop^{Ala2} RNAs, cleavage by the rhodium complex occurred specifically at a G·U mismatch, as well as at an exposed G residue in the larger loop region. In both the cases, strand scission occurred on the destacked side of the G·U mismatch at the residue on the 3' side of the U. Cleavage occurred at a C residue on the tRNA^{Ala} model RNAs, but previous studies showed that this 3' residue can also be a purine [9]. Similarly, FMN and light reactions led to cleavage on the 3' side of U of a G·U mismatch, and were independent of the 3' nucleotide composition [10]. In contrast, NiCR-induced strand scission required a uridine at the 3' side of the U of the G·U pair [7]. Crystal structures of RNAs containing intrahelical G·U mismatches reveal a high degree of stacking between the G·U pair and the Watson–Crick pair on the 5' side of uridine, and a destacked arrangement on the 3' side of uridine [12,14]. This unique stacking arrangement appears to be well suited for interactions with planar molecules or ligands such as NiCR, FMN, or $Rh(DIP)_3^{3+}$, although it has also been demonstrated that sulfate radicals may be able to carry out similar reactions [7]. Therefore, the ribose conformation at the 3' adjacent site must also be optimal in order for the abstraction of sugar protons to occur and lead to direct strand scission. The fact that $Rh(DIP)_3^{3+}$, FMN, and NiCR display slight variations in their cleavage specificities (e.g., preference for a specific residue on the 3' side of U) at the G·U sites suggests that they interact differently with the base mismatch, and that strand scission proceeds via different mechanisms. Bound magnesium ions at G·U mismatches may also play a role in cleavage specificity for these reagents as well as for the $CoCl_2/KHSO_5$ complex that generates reactive sulfate radicals. Further experimentation is clearly necessary in order to resolve these issues. Nonetheless, the results presented here and elsewhere [7,10]

demonstrate the utility of cleaving agents in identifying or comparing mismatch sites or other structural motifs.

In addition to cleavage adjacent to G·U pairs, NiCR also induces strand scission at exposed guanines, but in these cases, cleavage generally occurs through a base-oxidation pathway and requires alkaline treatment to reveal the reactive sites [7]. $Rh(DIP)_3^{3+}$ was shown previously to induce strand scission at an exposed G residue in a microhelix^{Phe} RNA [9] and cleaves at a related site on both the microhelix^{Ala} and 790-loop RNAs. This cleavage site was difficult to observe on the microhelix^{Ala} RNA because of nuclease damage in the loop region. Cleavage at the exposed G791 on the 790 loop is clearly observed, however, and is intriguing because G791 is one of the most highly conserved residues in 16S rRNA [19] and has been shown to be essential in genetic studies [20].

Recent crystal structures of the ribosome reveal that G791 is in close proximity to the decoding region and tRNAs in the E and P sites [34], and likely plays an important functional role. It is perhaps not surprising, then, that a single mutation at G791 leads to complete loss in function of the ribosome (P.R. Cunningham, K.-S. Lee, unpublished data). The 3 Å-resolution structure of the 30S subunit from *Thermus thermophilus* reveals a sharp turn in the 790 loop involving G791 [21]. A similar structure was observed by NMR (J. SantaLucia Jr., S. Varma, unpublished data), which also shows that the G791 residue is exposed to solvent and exhibits dynamic exchange between *anti* and *syn* conformations. The dynamic nature of the 790 loop may be important for its function, particularly with respect to protein synthesis, which is a dynamic process and involves movement of ribosomal RNA and contacts with mobile tRNAs and mRNA [34]. Thus, cleavage at this important G site may be reflective of an alternate sugar conformation (a mixture of C2'-*endo* and C3'-*endo* sugar puckers at G791) that is particularly sensitive to the metal complex. Also of note is the fact that the microhelix^{Ala} loop represents a tRNA anticodon loop and its sequence is similar to the 790 loop on the 5' side (5' UAG 3'); both regions are known to contact the decoding region of 16S rRNA. Thus, the similar rhodium-induced strand breaks at the G residues in the 790 loop (on both the small 17-nucleotide RNA and full-length 16S rRNA) and microhelix^{Ala} may be significant.

A related RNA hairpin structure has been reported for the iron responsive element (IRE) RNA [35,36]. Interestingly, the IRE hairpin has a six-nucleotide loop that has hydrogen-bonding interactions across the loop and contains a distinctive flipped-out residue on the 3' side of the loop. A functionally important loop G residue adopts a *syn* conformation and is solvent exposed. Ciftan et al. [37] reported that the exposed loop G residue in IRE, which resembles G791, is reactive towards an oxoruthenium(IV) compound that oxidizes guanines at solvent accessible sites. In general, six- or seven-nucleotide hairpin loops might be expected to exhibit conformational flexibility. However, nucleotide bases can participate in hydrogen-bonding interactions

across the loop and lead to increased stability of the loop. Such interactions may lead to unusual sugar–phosphate backbone structures and create highly reactive sites for the metal complexes. Alternatively, loop flexibility and dynamics may be important for long-range interactions or for RNA–RNA contacts in the RNA, and the metal complexes may be able to “recognize” such regions.

4.2. Relationship to RNA stability

In order to determine if any correlation exists between rhodium-induced cleavage and RNA stability, the ΔG_{37}^0 values of the mismatch sequence variants are compared (Table 1). For microhelix, tetraloop, and 790-loop RNAs, the G•U mismatch is less stable than the Watson–Crick base pairs by ~ 2 – 3 kcal/mol, but more stable than other mismatches by >1.5 kcal/mol (Table 1) [20,33]. No cleavage by the rhodium complex was observed at any mismatch site other than G•U, including the isostructural A⁺•C pair. The A•C pair is generally about 1.5–2 kcal/mol less stable than a G•U pair, but approximately equal in stability at lower pH. The structure of the protonated form of the A•C pair is shown in Fig. 2 and compared to the G•U mismatch structure. The G•U wobble pair contains two imino proton to carbonyl hydrogen bonds. Similarly, the protonated A•C pair contains two hydrogen bonds, the first between the cytidine N3 and adenosine G-amino proton, and the second between the cytidine 2-carbonyl and adenosine N1-imino proton. As supported by the NMR structure, the neighboring U788–A794 pair forms in the G•U and A•C 790-loop RNAs, as well as other mismatch-containing 790-loop RNAs [20]. In this study, we observed weak cleavage at G797 on the A⁺•C variant of the 790 loop (Fig. 4b) that is not observed on the G•U or on other mismatch RNAs. These results suggest that the A•C and G•U variants likely have different structures and/or chemical reactivities (which could arise from different structural environments), and that stability does not play a major role in the binding and subsequent cleavage specificity of Rh(DIP)₃³⁺.

In addition, rhodium-induced cleavage occurred specifically at G791 on all of the 787•795 mismatch variants of the 790 loop examined (G•U, A•C, U•G, U•U, C•U, and C•G), except for A•A. In contrast, we observed multiple cleavages on the A•A 790-loop variant. The one-dimensional NMR

studies revealed that this RNA was conformationally dynamic, as well as being the least stable 790 variant, but was also the most functional mutant [20]. The remaining mismatch RNAs (G•U, A•C, U•G, U•U, C•U, and C•G) differ in their thermodynamic stabilities (Table 1) [20], and only G•U, A•C, and C•U exhibit a U788–A794 pair as determined by one-dimensional imino proton NMR (data not shown). Therefore, little correlation can be made between RNA stability and cleavage by the metal complex. The rhodium compound is more likely detecting a specific RNA structure or sugar conformation at G791 that is conserved, even in the absence of a stable U788–A794 pair. The X-ray structure of the 30S ribosome [21] reveals that even in the absence of a strongly hydrogen-bonded A•C pair, the RNA loop structure is similar to that observed by solution NMR in which G791 and U793 are solvent exposed. The G residue is phylogenetically conserved and invariant and among all organisms, essential for function in vivo, and the structure may be conserved even when the loop-closing residues U788–A794 and 787•795 are varied.

4.3. Recognition and cleavage of G•U and novel G motifs in 16S rRNA by Rh(DIP)₃³⁺

Cleavage by Rh(DIP)₃³⁺ occurs on the 3' side of the uridine of intrahelical G•U mismatches in microhelix^{Ala}, tetraloop^{Ala2}, and 790-loop RNAs, as well as on yeast tRNA^{Phe}, yeast tRNA^{Asp}, and a microhelix^{Phe} RNA [9]. Cleavage at exposed G residues was also observed on these RNAs. Strand scission at G791 was observed on small RNAs representing the 790 loop of 16S rRNA and on the full-length 16S rRNA isolated from *E. coli*, suggesting that a similar conformation exists for both RNA loops. Similarly, the same result on the 17-nucleotide A•C variant and full-length 16S rRNA was obtained; no cleavage on the 3' side of the pyrimidine base of the A•C mismatch occurs. Thus, the rhodium probing data are consistent with the X-ray data and with the NMR of the 17-nucleotide A•C variant at pH 7.0, which reveal that the A787•C795 mismatch has a different structure than the G787•U795 mismatch observed by NMR. Both RNA conformations observed by X-ray [21] and NMR [20] studies may be important, however, and occur at different steps of translation in the ribosome.

Table 1
Comparison of RNA hairpin thermodynamics [20,33].

Microhelix RNA (3•18)	$\Delta\Delta G_{37}^0$ (kcal/mol) ^a (G•U–X•Y)	Tetraloop RNA (3•10)	$\Delta\Delta G_{37}^0$ (kcal/mol) ^a (G•U–X•Y)	790 loop RNA (787•795)	$\Delta\Delta G_{37}^0$ (kcal/mol) ^a (G•U–X•Y)
G•C	+2.4	G•C	ND	G•C	+3.3
A•C	–1.5	A•C	–1.6	A•C	–1.7
A ⁺ •C	ND	A ⁺ •C	+0.5	A ⁺ •C	–0.1
U•U	–1.7	U•U	–2.5	U•U	–1.6
C•U	ND	C•U	ND	C•U	–2.0
A•A	ND	A•A	ND	A•A	–2.1

^a The buffer conditions were 15 mM NaCl, 20 mM sodium cacodylate, and 0.2 (790 loop) or 0.5 (microhelix and tetraloop) mM Na₂EDTA, at pH 7.0 or 5.3 (for A⁺•C). ND, not determined.

Two additional sites of cleavage by $\text{Rh}(\text{DIP})_3^{3+}$ were observed on the full-length 16S rRNA. Strand scission occurred at G800 and G803 to give reverse-transcriptase stops at U801 and U804. Residue U804 participates in a G·U wobble pair with G778, thus, cleavage occurs on the 5' side of the U of the mismatch pair. This pattern is in contrast to previous cleavages on the destacked side (3' side of U) of the wobble pair. However, this mismatch is located at the end of a helical region, whereas the previous G·U pairs examined were intrahelical. Our results suggest that the stacking arrangement or geometry of this G·U site differs from the intrahelical G·U pairs. Furthermore, the X-ray structure reveals that this G·U pair lies in a region of highly unusual tertiary structure, which may also influence the structure at the G·U site [21]. The second cleavage site in this region at G800 was also shown in the X-ray structure to be involved with a non-canonical base-pairing interaction with A782 [21]. Further studies are currently in progress to understand better the structural and functional significance of these recognition sites.

5. Conclusions

A variety of chemical probes with different specificities can be employed to gain a greater knowledge of RNA secondary and tertiary structures. This information is helpful in determining the biological roles or significance of certain structural motifs, such as base mismatches or exposed residues, as well as offering assistance in simply assigning regions of double- or single-stranded RNA. In combination with classical alkylating agents such as dimethylsulfate and hydrazine, much more complementary information can be gleaned that will ultimately be helpful in determining the high-resolution X-ray or NMR structures of large RNAs and their complexes. In addition, many of the known chemical cleaving agents are being further developed and applied to study the structures of very large RNAs, as well as probing RNA structure in ribosomes or for in vivo determination of RNA structure.

Acknowledgements

Financial support was provided by the NIH (GM54632 to C.S. Chow; GM55745 and GM52896 to P.R. Cunningham and J. SantaLucia Jr.) and Wayne State University.

References

[1] D.W. Celander, T.R. Cech, Visualizing the higher order folding of a catalytic RNA molecule, *Science* 251 (1991) 401–407.
 [2] G.J. Murakawa, C.H.B. Chen, M.D. Kuwabara, D.P. Nierlich, D.S. Sigman, Scission of RNA by the chemical nuclease of 1,10-phenanthroline-copper ion: preference for single-stranded loops, *Nucleic Acids Res.* 17 (1989) 5361–5375.

[3] C.S. Chow, J.K. Barton, Shape-selective cleavage of tRNA^{Phe} by transition-metal complexes, *J. Am. Chem. Soc.* 112 (1990) 2839–2841.
 [4] C.S. Chow, J.K. Barton, Transition metal complexes as probes of nucleic acids, *Methods Enzymol.* 212 (1992) 219–242.
 [5] P.J. Carter, C.C. Cheng, H.H. Thorp, Oxidation of DNA and RNA by oxoruthenium(IV) metallointercalators: visualizing the recognition properties of dipyrrophenazine by high-resolution electrophoresis, *J. Am. Chem. Soc.* 120 (1998) 632–642.
 [6] H.H. Thorp, R.A. McKenzie, P.N. Lin, W.E. Walden, E.C. Theil, Cleavage of functionally relevant sites in ferritin mRNA by oxidizing metal complexes, *Inorg. Chem.* 35 (1996) 2773–2779.
 [7] R.P. Hickerson, C.D. Watkins-Sims, C.J. Burrows, J.F. Atkins, R.F. Gesteland, B. Felden, A nickel complex cleaves uridine in folded RNA structures: application to *E. coli* tmRNA and related engineered molecules, *J. Mol. Biol.* 279 (1998) 577–587.
 [8] I.J. Brittain, X. Huang, E.C. Long, Selective recognition and cleavage of RNA loop structures by Ni(II)-Xaa-Gly-His metallopeptides, *Biochemistry* 37 (1998) 12113–12120.
 [9] C.S. Chow, J.K. Barton, Recognition of G-U mismatches by tris(4,7-diphenyl-1,10-phenanthroline)rhodium(III), *Biochemistry* 31 (1992) 5423–5429.
 [10] P. Burgstaller, T. Hermann, C. Huber, E. Westhof, M. Famulok, Isoalloxazine derivatives promote photocleavage of natural RNAs at GU base pairs embedded within helices, *Nucleic Acids Res.* 25 (1997) 4018–4027.
 [11] P. Burgstaller, M. Famulok, Flavin-dependent photocleavage of RNA at GU base pairs, *J. Am. Chem. Soc.* 119 (1997) 1137–1138.
 [12] H. Mizuno, M. Sundaralingam, Stacking of Crick wobble pair and Watson-Crick pair: stability rules of G-U pairs at ends of helical stems in tRNAs and the relation to codon-anticodon wobble interaction, *Nucleic Acids Res.* 5 (1978) 4451–4461.
 [13] D. Gautheret, D. Konings, R.R. Gutell, G-U base pairing motifs in ribosomal RNA, *RNA* 1 (1995) 807–814.
 [14] D. Moras, P. Dumas, E. Westhof, GU base pairs and variable loop in yeast tRNA^{Asp}, *NATO ASI Ser., Ser. A* 110 (1986) 113–124.
 [15] W.H. McClain, K. Foss, Changing the identity of a tRNA by introducing a G-U wobble pair near the 3' acceptor end, *Science* 240 (1988) 793–796.
 [16] Y.M. Hou, P. Schimmel, A simple structural feature is a major determinant of the identity of a transfer RNA, *Nature* 333 (1988) 140–145.
 [17] S.A. White, H. Li, Yeast ribosomal protein L32 recognizes an RNA G:U juxtaposition, *RNA* 2 (1996) 226–234.
 [18] S.A. Strobel, T.R. Cech, Minor groove recognition of the conserved G-U pair at the *Tetrahymena* ribozyme reaction site, *Science* 267 (1995) 675–679.
 [19] R.R. Gutell, Collection of small subunit (16 S- and 16 S-like) ribosomal RNA structures, *Nucleic Acids Res.* 22 (1994) 3502–3507.
 [20] K.S. Lee, S. Varma, J. SantaLucia Jr, P.R. Cunningham, In vivo determination of RNA structure-function relationships: analysis of the 790 loop in ribosomal RNA, *J. Mol. Biol.* 269 (1997) 732–743.
 [21] B.T. Wimberly, D.E. Brodersen, W.M. Clemens Jr, R.J. Morgan-Warren, A.P. Carter, C. Vornheim, T. Hartsch, V. Ramakrishnan, Structure of the 30S ribosomal subunit, *Nature* 407 (2000) 327–339.
 [22] M.R. Kirshenbaum, R. Tribolet, J.K. Barton, $\text{Rh}(\text{DIP})_3^{3+}$: a shape-selective metal complex which targets cruciforms, *Nucleic Acids Res.* 16 (1988) 7943–7960.
 [23] D.C. Capaldi, C.B. Reese, Use of the 1-(2-fluorophenyl)-4-methoxypiperidin-4-yl (Fpmp) and related protecting groups in oligoribonucleotide synthesis: stability of internucleotide linkages to aqueous acid, *Nucleic Acids Res.* 22 (1994) 2209–2216.

- [24] N. Usman, K.K. Ogilvie, M.Y. Jiang, R.J. Cedergren, Automated chemical synthesis of long oligoribonucleotides using 2'-*O*-silylated ribonucleoside 3'-*O*-phosphoramidites on a controlled-pore glass support: synthesis of a 43-nucleotide sequence similar to the 3'-half molecule of an *Escherichia coli* formylmethionine tRNA, *J. Am. Chem. Soc.* 109 (1987) 7845–7854.
- [25] E.G. Richards, Use of tables in calculation of absorption, optical rotary dispersion, and circular dichroism of polyribonucleotides, in: G.D. Fasman (Ed.), *Handbook of Biochemistry and Molecular Biology: Nucleic Acids*, CRC Press, Cleveland, 1975, pp. 596–599.
- [26] T.E. England, A.G. Bruce, O.C. Uhlenbeck, Specific labeling of 3' termini of RNA with T4 RNA ligase, *Methods Enzymol.* 65 (1980) 65–74.
- [27] D.A. Peattie, Direct chemical method for sequencing RNA, *Proc. Natl. Acad. Sci. USA* 76 (1979) 1760–1764.
- [28] T. Powers, H.F. Noller, A functional pseudoknot in 16S ribosomal RNA, *EMBO J.* 10 (1991) 2203–2214.
- [29] S. Stern, D. Moazed, H.F. Noller, Structural analysis of RNA using chemical and enzymatic probing monitored by primer extension, *Methods Enzymol.* 164 (1988) 481–489.
- [30] C. Francklyn, P. Schimmel, Aminoacylation of RNA minihelices with alanine, *Nature* 337 (1989) 478–481.
- [31] J.P. Shi, S.A. Martinis, P. Schimmel, RNA tetraloops as minimalist substrates for aminoacylation, *Biochemistry* 31 (1992) 4931–4936.
- [32] C.S. Chow, L.S. Behlen, O.C. Uhlenbeck, J.K. Barton, Recognition of tertiary structure in tRNAs by Rh(phen)₂phi³⁺, a new reagent for RNA structure-function mapping, *Biochemistry* 31 (1992) 972–982.
- [33] M. Meroueh, C.S. Chow, Thermodynamics of RNA hairpins containing single internal mismatches, *Nucleic Acids Res.* 27 (1999) 1118–1125.
- [34] M.M. Yusupov, G.Z. Yusupova, A. Baucom, K. Lieberman, T.N. Earnest, J.H. Cate, H.F. Noller, Crystal structure of the ribosome at 5.5 Å resolution, *Science* 292 (2001) 883–896.
- [35] L.G. Laing, K.B. Hall, A model of the iron responsive element RNA hairpin loop structure determined from NMR and thermodynamic data, *Biochemistry* 35 (1996) 13586–13596.
- [36] K.J. Address, J.P. Basiion, R.D. Klausner, T.A. Rouault, A. Pardi, Structure and dynamics of the iron responsive element RNA: implications for binding of the RNA by iron regulatory binding proteins, *J. Mol. Biol.* 274 (1997) 72–83.
- [37] S.A. Ciftan, E.C. Theil, H.H. Thorp, Oxidation of guanines in the iron-responsive element RNA: similar structure from chemical modification and recent NMR studies, *Chem. Biol.* 5 (1998) 679–687.